Journal of Materials Chemistry A

Accepted Manuscript

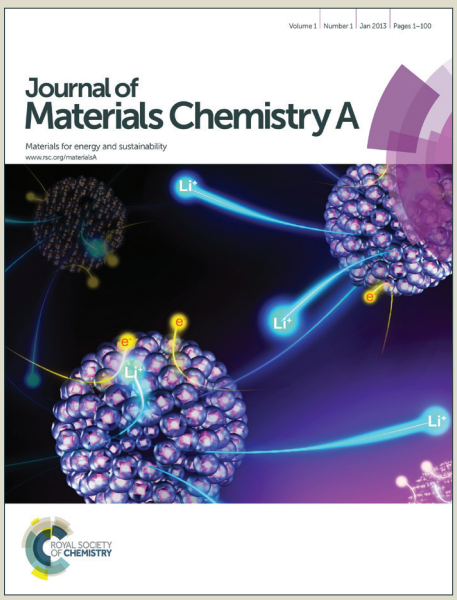

ROYAL SOCIETY OF CHEMISTRY

www.rsc.org/materialsA

Graphical abstract

Ranran Zhang, Yanyan He and Liqiang Xu*

Controllable synthesis of hierarchical $ZnSn(OH)_6$ and Zn_2SnO_4 hollow nanospheres and their applications as anodes for lithium ion batteries

Hierarchical $ZnSn(OH)_6$ hollow nanospheres that are composed of nanorods have been conveniently prepared via a simple hydrothermal process at 180 °C for 24 h in the presence of polyacrylic acid (PAA, acts as an in-situ template role). It is interesting to find that they could convert into hierarchical Zn_2SnO_4 hollow nanospheres after subsequent calcinations. The good reversible character and excellent electrochemical performances of the as-obtained hierarchical $ZnSn(OH)_6$ and Zn_2SnO_4 hollow nanospheres enable them to be promising and competitive high-performance anodes for Lithium ion batteries.

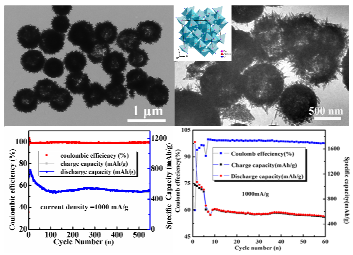

Cite this: DOI: 10.1039/c0xx00000x

www.rsc.org/xxxxxx

ARTICLE TYPE

Controllable synthesis of hierarchical $ZnSn(OH)_6$ and Zn_2SnO_4 hollow nanospheres and their applications as anodes for lithium ion batteries

Ranran Zhang, Yanyan He and Liqiang Xu*

Received (in XXX, XXX) Xth XXXXXXXXX 20XX, Accepted Xth XXXXXXXXX 20XX

DOI: 10.1039/b000000x

Hierarchical $ZnSn(OH)_6$ hollow nanospheres that are composed of nanorods have been conveniently prepared via a simple hydrothermal process at 180 °C. It is interesting to find that they could convert into hierarchical Zn_2SnO_4 hollow nanospheres after subsequent calcinations. The as-obtained $ZnSn(OH)_6$ and Zn_2SnO_4 deliver initial discharge capacity of 2197.4 and 1618.2 mAh g^{-1} at 100 mA g^{-1}, and maintain a reversible specific capacity of 801.2 (after 60 cycles) and 602.5 mAh g^{-1} (after 60 cycles), respectively; It is note that even if the current density was set as high as 1A g^{-1}, they still could maintain reversible specific capacity of 741.9 (after 1000 cycles) and 442.8 mAh g^{-1} (after 60 cycles). The facile synthesis, high specific capacity, good cycling stability and high rate performance of the as-obtained hierarchical $ZnSn(OH)_6$ and Zn_2SnO_4 hollow nanospheres enable them to be promising and competitive high-performance anodes for LIBs.

I. Introduction

Hierarchical hollow nanosphere has long been a focus of research during the past few decades owing to its well-defined morphology, uniform size, low density and synergetic effect of components. It has a rich variety of tunable physicochemical properties and has wide range of potential applications in medicine, biological molecules, catalysts, energy related research areas etc.[1-3] The facile design and application of hierarchical hollow nanosphere architecture that are consisting of low dimensional nanoscale building blocks (such as nanorods) has been chosen as one of the most effective way for the further improvement of the cycling and rate performances of electrodes for lithium ion batteries (LIBs),[4, 5] because its hollow structure usually could facilitate the penetration of the electrolyte into the electrode and accommodate the volume swing generated during the Li^+ intercalation/extraction process, in addition, the one-dimensional (1D) building blocks have high surface area, novel size effects, and significantly enhanced kinetics for Li^+ transportation, which usually resulting in good cycling stability and high specific capacity of the overall electrode. Up to date, a series of anode materials with hierarchical hollow spherical architectures, such as SnO_2,[3, 6] Co_3O_4,[7] V_2O_5,[8] NiS[9] and α-Fe_2O_3[10] etc. with enhanced capacity and cycle performances have been reported by different groups worldwide. Their higher capacity and stability compared with those of the solid or individual structured nanomaterials are largely attributed to the synergistic effect of the stable hollow structures and low dimensional nanoscale building blocks on the accommodation of volume change and the reduction of the diffusion path of electron/Li-ions.[1, 2]

Up to date, extensive research has been devoted to tin based composites owing to their unique structures and special properties, [1, 6, 11] for example, inverse spinel-type Zn_2SnO_4 is one of the most promising negative-electrode tin based materials for lithium ion batteries due to its ability to react with up to 8 Li^+ ions per formula unit, which gives a theoretical capacity of 1231 mAh g^{-1}.[12] In recent years, many Zn_2SnO_4 individual nanostructures including solid cube, hollow cube, octahedral, nanoneedles and nanowires [13-17] have all been synthesized and studied as anode materials. In addition, Zn_2SnO_4 nanocomposites such as Zn_2SnO_4/C, Zn_2SnO_4/graphene, Zn_2SnO_4/PPy, Zn_2SnO_4/PANI as well as Zn_2SnO_4/ZIF were also studied.[18-20] Although obvious improvements have been made in these reported works, the poor cyclability and poor rate performance of Zn_2SnO_4 caused by the volume change during the insertion/extraction of Li ions and poor conductivity, still remain a great challenge to be overcome. Therefore, design and tailor Zn_2SnO_4 hierarchical hollow structures might be an appealing choice to address the challenge, while $ZnSn(OH)_6$ is an proper precursor for the formation of Zn_2SnO_4. To the best of survey, though $ZnSn(OH)_6$ has been widely used as photocatalyst, flame retardant and smoke suppression agent,[21] the application of $ZnSn(OH)_6$ as an advanced anode material has rarely been reported until now.

In this study, $ZnSn(OH)_6$ hollow nanospheres that are composed of nanorods with diameters in the range of 40-80 nm have been successfully prepared by adding PAA in the hydrothermal process. It is found that PAA acts as in-situ template role during the formation of $ZnSn(OH)_6$ hollow nanospheres. It is interesting to find that hierarchical Zn_2SnO_4 hollow nanospheres could be obtained only by the pyrolysis of $ZnSn(OH)_6$ hollow nanospheres. Both of the $ZnSn(OH)_6$ and Zn_2SnO_4 hollow nanospheres deliver high initial discharge

capacities and excellent rate performances. The former can maintain a reversible specific capacity of 801.2 mAh g^{-1} after 60 cycles, while the latter could retain at 602.5 mAh g^{-1} after 60 cycles at 100 mA g^{-1}. It is note that even if its current density was set as high as 1A g^{-1}, they still could maintain reversible specific capacity of 741.9 mAh g^{-1} (after 1000 cycles) and 442.8 mAh g^{-1} (after 60 cycles), respectively. The excellent electrochemical performance of these electrodes can be attributed to the hollow interconnected hierarchical nanostructures, which prevent the self-agglomeration of he electrode materials and buffer their volume change during the discharge–charge process. To the best of our knowledge, this is the first report about the performance of hierarchical $ZnSn(OH)_6$ and Zn_2SnO_4 hollow nanospheres nanostructures as anode materials for LIBs. The facile synthesis, high specific capacity, good cycling stability, and high rate performance of the as-obtained hierarchical $ZnSn(OH)_6$ and Zn_2SnO_4 hollow nanospheres enable them to be the promising and competitive anode materials for the high-performance LIBs.

II. Experimental section

A. Preparation of the hierarchical $ZnSn(OH)_6$ hollow nanospheres

All the reagents used here were of analytical grade without further purification. In a typical synthesis procedure, a solution with 0.439 g of $Zn(CHCOO)_2{\cdot}2H_2O$, different amounts of PAA (0.25 g, 0.50 g, 0.75 g, 1.00g) was separately dissolved in 25 mL of deionized water under magnetic stirring for 30 min at room temperature. Then, 0.18 M $Na_2SnO_3{\cdot}4H_2O$ (10 mL) was added into the above solution. After it was stirred for 15 min, 6 mL $NH_3{\cdot}H_2O$ were dropped slowly. Finally, the mixed solution was continually stirred for 30 min before it was transferred into a Teflon-lined autoclave with a capacity of 60 mL. The autoclave was heated from room temperature to 180 ℃ and maintained at 180 ℃ for 24 h. The product of hollow $ZnSn(OH)_6$ nanospheres were collected by centrifugation and washed repeatedly with anhydrous ethanol and distilled water for several times, and then it was dried in vacuum at 60°C for 12 h.

B. Preparation of the hierarchical Zn_2SnO_4 hollow spheres

The as-obtained $ZnSn(OH)_6$ product (produced with the amount of PAA is 0.75 g) was annealed at 600 ℃ (with a increasing heating rate of 5 ℃ min^{-1}) in air for 6 h in a tube furnace, then cooled to room temperature naturally.

C. Material characterization

X-ray powder diffraction (XRD) patterns of the sample were obtained from a Bruker D8 advanced X-ray diffractometer that was equipped with graphite-monochromated $Cu_{K\alpha}$ radiation (λ = 1.5418Å). The Fourier transform infrared spectroscopy (FT-IR) spectrum instrument used here was a Bruker VERTEX 70 with a resolution of 4 cm^{-1}. TEM images were taken on a JEM-2100 microscope. The high resolution images were recorded using a high resolution transmission electron microscope (HRTEM, JEOL-2100F) operated at 200 kV. Particle morphology images were recorded using a field-emission scanning electron microscope (FESEM, JEOL JSM-6700 M) with energy-dispersive X-ray (EDX) spectroscopy and an EDX mapping system (30 kV). The BET surface area (SBET) and Barrett–Joyner–Halenda (BJH) pore size distribution (PSD) were characterized by a QuadraSorb SI surface area analyzer (version 5.06); Surface analysis of the studied samples was performed using XPS (VGESCA-LABMK X-ray photoelectronic spectrometer).

The electrochemical discharge-charge performances of the samples were tested on a Land battery test system (CT2001A) at 25°C. The working electrodes were consisted of 75 wt% active materials [hierarchical $ZnSn(OH)_6$ or Zn_2SnO_4 hollow nanospheres], 15 wt% carbon black, and 10 wt% CMC. Distilled water was used as the solvent. The mixed slurry with thickness of 200 μm was coated onto a piece of copper foil and dried in vacuum oven at 60°C for 12 h, then cut into discs with diameter of 12 mm. And the mass calculation of the active Zn_2SnO_4 materials was carried out based on 75% of the mass of electrode piece. Copper foil was used as the current collector, and Celgard 2300 microporous polypropylene membrane was used as the separator. The electrolyte was composed of 1 mol/L $LiPF_6$ dissolved ethylene carbonate/dimethyl carbonate/diethyl carbonate (EC/DMC/DEC, volume ratio was 1:1:1). Lithium foils with the diameter of 15 mm and the thickness of 0.4 mm were used as the counter electrodes. The button batteries were assembled in an argon-filled glove box, and cycled at different charge-discharge current densities (100, 500, 1000 mA g^{-1}) within voltage limit of 0.01V-3.00V using a Land battery test system (CT2001A, China) at room temperature (25 °C).

III. Results and Discussions

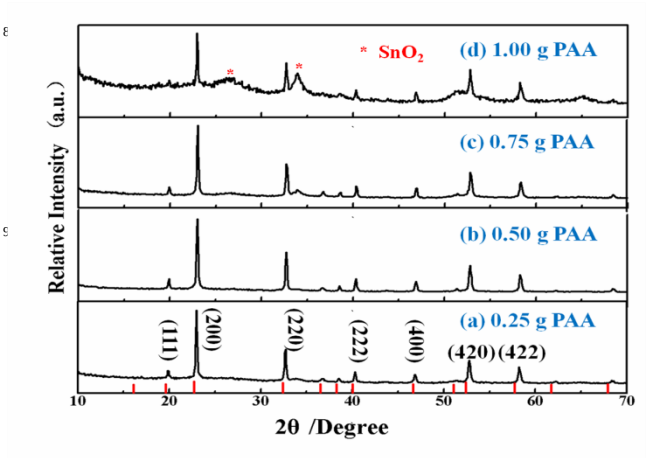

Fig. 1 Typical XRD patterns of the $ZnSn(OH)_6$ obtained using different amounts of PAA.

Typical XRD patterns of the as-prepared $ZnSn(OH)_6$ products using different amounts of PAA are presented in Fig. 1. It is clear that all of the diffraction peaks with high diffraction intensity in Fig. 1(a-c) can be indexed to the cubic $ZnSn(OH)_6$ (JCPDS card no. 20-1455; a=b=c=7.800 Å), and no diffraction peaks of impurities are observed, indicating high purity and good crystallinity of the products. However, it is find that $ZnSn(OH)_6$ co-existed with SnO_2 were obtained (in Fig. 1d, marked with the star sign) when the using amount of PAA is 1.00 g. The formation of $ZnSn(OH)_6$ can be described by the following reaction equations:

$$NH_3{\cdot}H_2O \rightarrow NH_4^+ + OH^-$$
$$SnO_3^{2-} + 3\,H_2O \rightarrow Sn(OH)_6^{2-}$$
$$Zn^{2+} + Sn(OH)_6^{2-} \rightarrow ZnSn(OH)_6$$

Fig. 2 show the FESEM and TEM images of the as-obtained $ZnSn(OH)_6$ products obtained using different amounts of PAA. It is observed that only irregular shaped small nanospheres [diameters: 50-120 nm, see Fig. 2 (a, e)] with rough surfaces and hollow inner cores are produced when the using amount of the PAA was 0.25 g; Increasing the amount of PAA to 0.50 g, irregular hollow nanospheres [diameters: 200-500 nm, see Fig. 2 (b, f)] with needle-like nanorods (lengths: 80-180 nm) observed on their surfaces were obtained; When the amount of PAA was increased to 0.75 g, the surfaces of the hollow nanospheres [diameters: 300-800 nm, Fig. 2 (c, g)] are uniformly covered with needle-like nanorods (lengths: 80-100 nm); Extending the amount of PAA to 1.00 g results in fall-off of the needle-like nanorods from the surfaces of the hierarchical $ZnSn(OH)_6$ hollow nanospheres. In comparison with the sample obtained when the amount of PAA is 0.75 and 1.00 g, the diameter ranges of the hollow $ZnSn(OH)_6$ nanospheres (Fig. 2d and 2h) are the same. It is also found that pure and well crystalline cubic $ZnSn(OH)_6$ (JCPDS card no. 20-1455) could still be obtained (Fig. S1a) in the absence of PAA, while only irregular hexagonal sheets and nanoneedles not hierarchical Zn_2SnO_4 hollow nanospheres were obtained under TEM observations [Fig. S1(b, c)]. Therefore, PAA play vital roles on both the morphology and size of the hierarchical Zn_2SnO_4 hollow nanospheres. Besides the PAA, it is found that their formation is also a time-dependent process (Fig. S2).

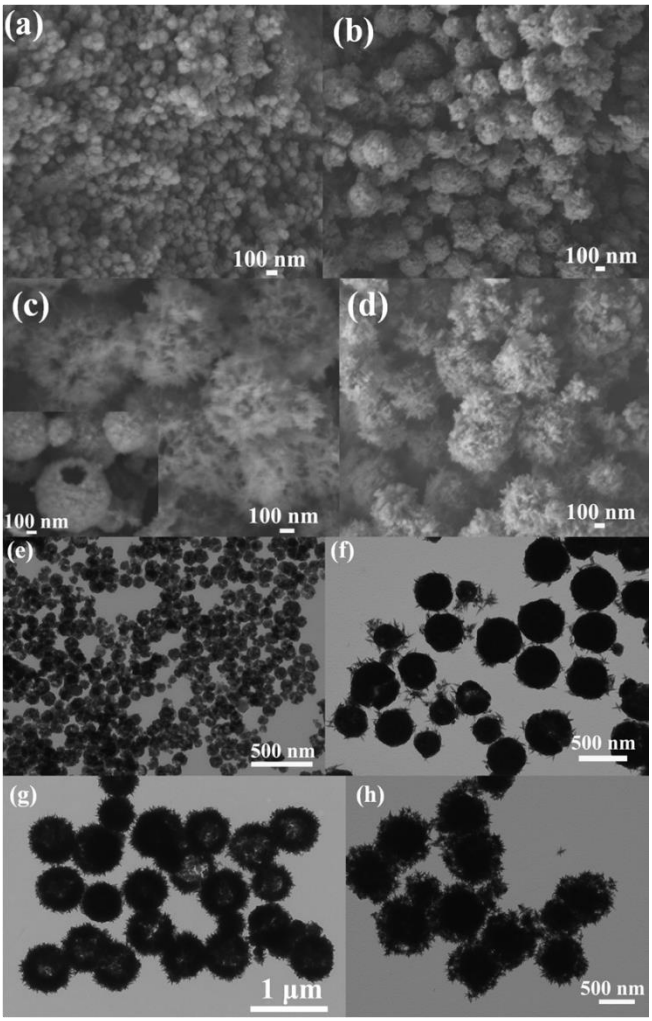

Fig. 2 FESEM and TEM images of the $ZnSn(OH)_6$ synthesized using different amounts of PAA: (a, e) 0.25 g; (b, f) 0.50 g; (c, g) 0.75 g; and (d, h) 1.00 g. Inset in Fig. 2 (c) shows an individual hollow $ZnSn(OH)_6$ nanosphere.

Table 1. Detailed results of the as-obtained $ZnSn(OH)_6$ products using different amounts of PAA while keeping other experimental parameters unchanged.

Amount of PAA (g)	Morphology of the as-obtained product	Average diameter of the hollow spheres (nm)	Lengths of the nanoneedles (nm)
0.25	hierarchical $ZnSn(OH)_6$ hollow spheres	50-120	no nanoneedles
0.50	hierarchical $ZnSn(OH)_6$ hollow spheres	200-500	80-180
0.75	hierarchical $ZnSn(OH)_6$ hollow spheres	300-800	80-100
1.00	hierarchical $ZnSn(OH)_6$ hollow spheres + SnO_2 impurities	300-800	50-200

From the above phenomena (the products have the similar hierarchical spherical morphology, but the sizes of spheres and secondary nanorods are changed at different stages) of the contrast experiments, it is considered that the formation of the final hierarchical Zn_2SnO_4 hollow nanospheres may be attributed to a dissolution-recrystallization process followed by Ostwald ripening (see Scheme 1) under hydrothermal synthesis.

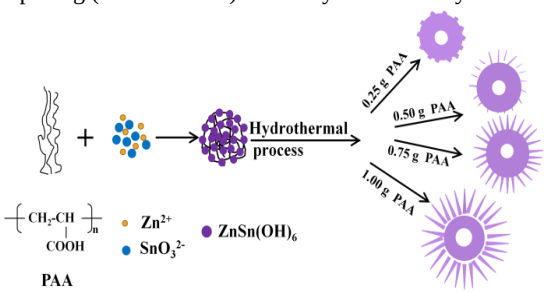

Scheme 1. Schematic illustration of the possible formation mechanism of the hierarchical hollow $ZnSn(OH)_6$ nanospheres.

The electrochemical properties of the as-obtained hierarchical hollow $ZnSn(OH)_6$ nanospheres (the using amount of PAA is 0.75 g) have been studied and the results are shown in Fig. 3. Fig. 3a displays the first 30th discharge/charge curves (i.e., voltage vs. capacity) at a current density of 100 mA g^{-1}. These hierarchical hollow $ZnSn(OH)_6$ nanospheres exhibit a large initial discharge capacity of 2197.4 mAh g^{-1} and show a very high reversible capacity of 801.2 mAh g^{-1} after 60 cycles [Fig. 3(a, b)] at 100 mA g^{-1}. Fig. 3d displays the discharge and charge capacity versus cycle number of the hierarchical $ZnSn(OH)_6$ hollow microspheres electrode at 500 mA g^{-1}, which exhibits a stable reversible capacity after 200 cycles. Except the first cycle (~ 1839.3 mAh g^{-1}), the rest 199 cycles almost maintained constant at ~ 680 mAh g^{-1}, indicating the high reversible capacity and good cycle life of the product. When the current density is set as high as 1A g^{-1}, the reversible discharge capacity could still be maintained at 741.9 mAh g^{-1} after 1000 cycles. The phenomenon of the capacity increasing with cycling has been found in many metal oxide anode materials. In our experiment, it may be ascribed to the

contributions of the pseudocapacitive interfacial storage, structure variations of the anode materials after long cycling and the decompositions of electrolyte etc., [22-24] however, the exact reason still needs further research. It is note that the hierarchical hollow $ZnSn(OH)_6$ nanosphere electrode exhibits the average discharge capacity of 1165, 847, 709, 603 mAh g^{-1} at the current densities of 100, 200, 500 and 1000 mAg^{-1} (Fig. 3f), respectively. To the best of our knowledge, it is found that the initial large irreversible capacity is almost inevitable for most reported anode materials. In this experiment, at the current density of 100 mAg^{-1}, the initial discharge and charge capacities are 2197.4 and 1033.9 mAh g^{-1}, corresponding to a coulombic efficiency of 66.62% and 47.05%, respectively. The capacity loss in the first cycle might be mainly attributed to the irreversible reduction of electrode active materials, the electrolyte decomposition and the formation of the solid electrolyte interface (SEI) layer. [25-27] When the current density restores to 100 mA g^{-1} after 10 cycles at 1 A g^{-1}, the cell recovers full charge capacity of 906 mAh g^{-1}, indicating the high cycle stability of the anodes in a wide range of current densities. The superior electrochemical performances of the $ZnSn(OH)_6$ product can be attributed to its large surface area, 3D hierarchical hollow nanosphere morphology, 1D nanorod subunit shape, which decreased the diffusion path and increased the effective space for insertion and extraction of Li ions.[28, 29]

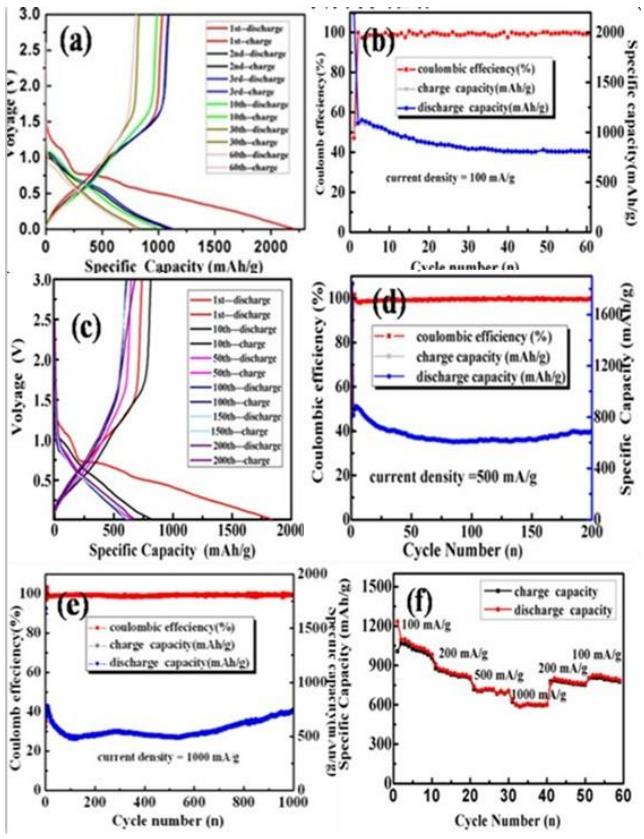

Fig. 3 (a-d) Typical discharge–charge curves of hierarchical hollow $ZnSn(OH)_6$ nanospheres for selected cycles at 100, 1000 mA g^{-1} and corresponding discharge/charge capacity and coulombic efficiency, respectively; (e, f) discharge/charge capacity and coulombic efficiency at 1000 mA g^{-1} and the rate performance of the hierarchical hollow $ZnSn(OH)_6$ nanospheres electrode.

A typical XRD pattern of the product obtained by calcining hierarchical $ZnSn(OH)_6$ hollow nanospheres (the amount of PAA is 0.75 g) is shown in Fig. 4a. The diffraction peaks that are indexed consistent well with the data of inverse spinel Zn_2SnO_4 with lattice constants a=8.657 Å, b=8.657 Å, and c=8.657 Å (JCPDF card no. 24-1470), while the peaks that are marked with star signs corresponding to the SnO_2. The calcined reaction mechanism may be described as follows according to the results of the above XRD pattern and weight loss of the product (see Fig. S3):

$$2ZnSn(OH)_6 \rightarrow Zn_2SnO_4 + SnO_2 + 6H_2O$$

The full nitrogen sorption isotherms of the Zn_2SnO_4 is presented in Fig. 4b, which gives an obvious hysteresis loop of type IV, suggesting the presence of macrospores. According to the investigative results, the hierarchical Zn_2SnO_4 hollow nanospheres give rise to a relatively high BET specific surface area of 42.53 $m^2 g^{-1}$ and a pore volume of 0.24 $cm^3 g^{-1}$, which is higher than the previous reported hollow Zn_2SnO_4 boxes and hollow Zn_2SnO_4@PPY. The porous structure of the Zn_2SnO_4 is a benefit for lithium intercalation and de-intercalation, which can also provide a high conductive medium for electron transfer. The surface purity of the as-obtained product after the calcinations of $ZnSn(OH)_6$ hollow nanospheres were investigated by the XPS spectrum, and the results evidence the formation of Zn_2SnO_4 and SnO_2 (Fig. S4), while no peaks that related with impurities have been detected.

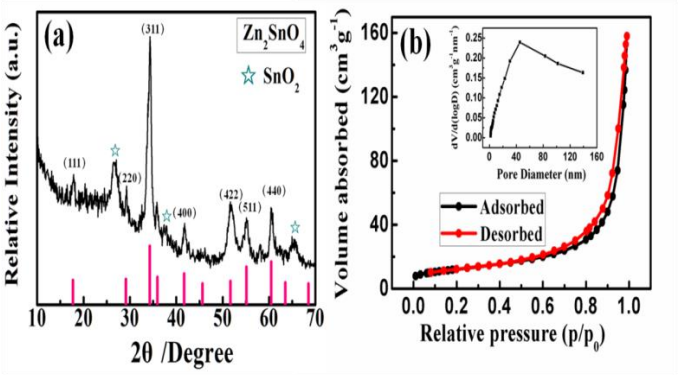

Fig. 4 (a) XRD pattern of the as-obtained Zn2SnO4 product and the corresponding standard XRD pattern; (b) Nitrogen adsorption–desorption isotherm and the corresponding pore size distribution (inset) of the hierarchical Zn2SnO4 hollow nanospheres.

Fig. 5 (a, b) show the low-magnification FESEM images of the final sample after calcinations of the hierarchical hollow $ZnSn(OH)_6$ nanospheres. It can be seen that hierarchical hollow spherical characteristics can be reserved after the conversion. A typical FESEM image (inset in Fig. 5b) of a nanosphere reveals its hollow characteristic feature. A typical TEM image of the hollow nanospheres is presented in Fig. 5c: the diameters of these nanospheres are in the range of 400-600 nm; The average length of the nanoneedles stood on the surface of nanospheres (with porous interiors that are composed of nanosized needle-like subunits) is about 100 nm. The typical TEM image of a single nanosphere in Fig. 5d clearly confirm the hierarchical hollow structure of the as-prepared Zn_2SnO_4 sample. The SAED pattern

of the inner core (circled by a big square) inset in Fig. 5d indicates the existence of SnO_2, and all the diffraction rings can be indexed to be (110), (101) and (211) of SnO_2, respectively. A representative HRTEM image of the area that marked with the small square in Fig. 5d is shown in Fig. 5e. The observed and calculated d-spacings from the HRTEM image are 0.31 and 0.23 nm, which match well with the corresponding d-spacings of the {220} and {111} facets of cubic Zn_2SnO_4. And the corresponding SAED pattern of the smaller square displays in Fig. 5f further evidencing the formation of Zn_2SnO_4 nanoneedles.

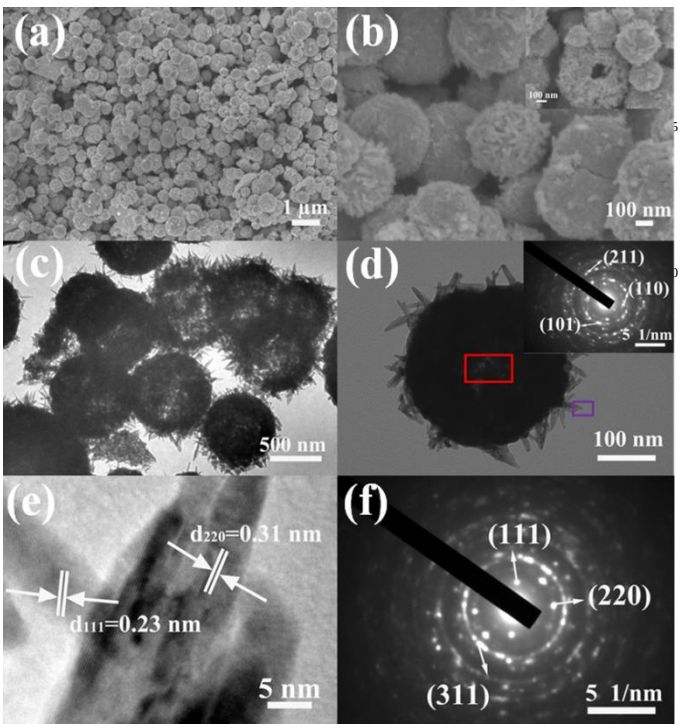

Fig. 5 (a, b) FESEM images of the hierarchical Zn_2SnO_4 hollow nanospheres at different magnifications, inset is a typical FESEM image of a hollow structured nanosphere; (c, d) TEM images of the final products and the corresponding SAED pattern marked with the bigger square in Fig. 5d; (e, f) HRTEM image and corresponding SAED pattern at the edge of a nanosphere that marked with the smaller square in Fig. 5d.

The discharge-charge curves in the first five cycles and the cycling performances of hollow Zn_2SnO_4 spheres (the using amount of PAA is 0.75 g) are displayed in Fig. 6a. And the results indicate that their first discharge-charge capacities are 1618.2 and 1070.7 mAh g^{-1} (see Fig. 6b) at the current density of 100 mA g^{-1} within 0.01-3.0 V. The irreversible capacity loss is 549.5 mAh g^{-1} with a coulombic efficiency of 66.2 %. For the 2nd cycle, the electrode shows a discharge capacity of 1093.5 mAh g^{-1} and the corresponding charge capacity of 1026.9 mAh g^{-1}, which exhibits a coulombic efficiency of 93.9%. The hierarchical hollow Zn_2SnO_4 nanospheres deliver a reversible discharge capacity as high as 602.5 mAh g^{-1} after the 60th cycle, which demonstrates their good charge–discharge cycling stability. The rate capability of the hierarchical hollow Zn_2SnO_4 spheres was evaluated at different current densities (Fig. 6c). At 100 mA g^{-1}, the Zn_2SnO_4 sample shows a 10th cycle specific capacity of 966.9 mAh g^{-1}. At a higher current density of 500 mA and 1000 mA g^{-1}, the specific capacity in the 10th cycle remained at 568.8 mAh g^{-1} and 470.8 mAh g^{-1}, respectively. When the current density returns to the initial 100 mA g^{-1}, the hollow Zn_2SnO_4 spheres recovered the average capacity of 628.1 mAh g^{-1}. Fig. 6 (d, e) show the cycling performances of the electrode at high current densities (500 and 1000 mA g^{-1}) between 0.01 and 3.0 V, respectively. It can be seen in Fig. 6d that the charge-discharge capacities of the sample maintained a stable trend before 60 cycles with a discharge capacity of 470.3 mAh g^{-1}. When the current density was increased to 1000 mA g^{-1} (Fig. 6e), the electrode can still retain a discharge capacity of 442.8 mAh g^{-1} for the 60th cycle approaching that of the one-dimensional Mn_3O_4 nanorod /Zn_2SnO_4 nanoneedle hierarchical composites,[30] demonstrating the excellent cycling stability of hollow Zn_2SnO_4 spheres as an anode material even at high current densities. These hierarchical Zn_2SnO_4 hollow nanospheres exhibit a higher capacity and superior stability compared to the previously reported cycling performances of Zn_2SnO_4 related materials (see Table 2). It is worth mentioning that the hierarchically hollow spherical structure of Zn_2SnO_4 are perfectly remained after 20th cycles at the current density of 500 mA g^{-1} (Fig. S5), further evidencing the excellent cycling stability of the as-obtained hierarchical Zn_2SnO_4 hollow nanospheres.

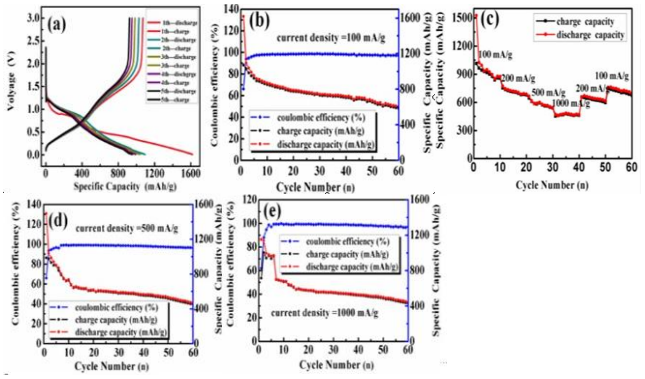

Fig. 6 (a, b) Typical discharge–charge curves of the as-obtained hierarchical hollow Zn_2SnO_4 nanospheres for selected cycles at 100 mA g^{-1} and corresponding discharge/charge capacity and coulombic efficiency curves; (c) The rate performance of the hierarchical hollow Zn_2SnO_4 nanosphere electrode; (d, e) discharge/charge capacity and coulombic efficiency at a current density of 500 and 1000 mA g^{-1}, respectively.

The as-obtained hierarchical $ZnSn(OH)_6$ and Zn_2SnO_4 hollow nanospheres all displaying excellent electrochemical performances (see Fig. 3, Fig. 6, Fig. 6 and Fig. S6), which might be largely attributed to their unique morphologies and structures: 1) The uniform pore size distribution of hollow nanostructures is easily accessible for electrolyte diffusion and intercalation of lithium ion into the active materials, which can short the lithium diffusion length and can provide more active sites for the extra lithium ions. It is the main reason why the cycle performance of hierarchical Zn_2SnO_4 hollow nanospheres is better than those of most reported Zn_2SnO_4 materials; It is considered that this is also the main reason for the high cycle performances of the as-obtained hierarchical hollow $ZnSn(OH)_6$ nanospheres; 2) The high surface area derived from the porous structures increases the electrolyte/materials contact area and reduces their contact

distance, resulting in enhanced electrochemical performance; 3) The hollow structures can supply extra spaces to sustain the volume changes of $ZnSn(OH)_6$ and Zn_2SnO_4 during the electrochemical cycles, and the porous structure is less prone to encounter structural collapse and possess improved rate capability and cycle stability; 4) The stable 1D nanorods stand on the surface of nanospheres seem to be favor for the prolonged cycle life of Sn-Zn-O anodes.

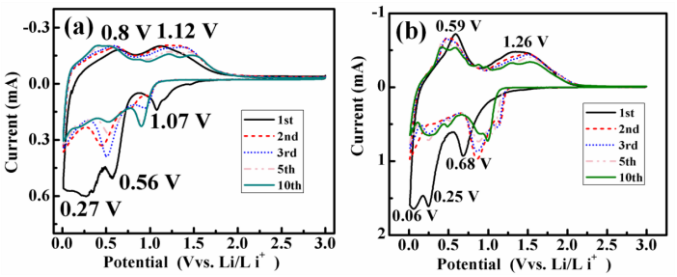

Fig. 7 Cyclic voltammograms of a) the hierarchically hollow $ZnSn(OH)_6$ nanospheres (obtained with 0.75g PAA) electrode; b) the hierarchically hollow Zn_2SnO_4 nanospheres electrode at a scan rate of 0.1 mV.S^{-1} in the region of 0.01-3.0 V (versus Li/Li^+).

Cyclic voltammetry is carried out on the hierarchically hollow $ZnSn(OH)_6$ and Zn_2SnO_4 nanosphere electrodes (with Li-metal as the counter and reference electrode) and the curves are shown in Fig. 7. Fig. 7a displays the first few complete cycles of $ZnSn(OH)_6$ electrode performed between 0.01-3.0 V at a scan rate of 0.1 mV s^{-1}, in the first cycle, the main reductive peaks are located at 0. 27, 0. 56 and 1. 07 V (Vs Li^+/Li), which might be attributed to the formation of solid electrode interphase (SEI) and partial crystal structure evolutions of the electrode materials. The two main oxidative peaks located at 0.8 and 1.12 V correspond to the delithiation processes of Li_xSn and Li_yZn and the decomposition of Li_2O; Fig. 7b displays the first few complete cycles of Zn_2SnO_4 electrode performed between 0.01-3.0 V at a scan rate of 0.1 mV s^{-1}. In the first cycle, the main reductive peaks are located at 0.06, 0.25 and 0.68 V (Vs Li^+/Li), which corresponds to the formation of solid electrode interphase (SEI) because of the reduction of organic solvents in the electrolyte, and partly crystal structure destruction (Eq. 1) followed by Li-alloying of Sn and Zn (Eqs. 2 and 3), meanwhile, two main oxidative peaks located at 0.59 and 1.26V correspond to the delithiation processes of Li_xSn and Li_yZn as described in Eqs. (2) and (3) and the decomposition of Li_2O.[31]

$$8Li^+ + Zn_2SnO_4 + 8e^- \rightarrow 2Zn + Sn + 4Li_2O \quad (1)$$

$$xLi^+ + Sn + xe^- \leftrightarrow Li_xSn \quad (0 \le x \le 4.4) \quad (2)$$

$$yLi^+ + Zn + ye^- \leftrightarrow Li_yZn \quad (y \le 1) \quad (3)$$

The peak current and the integrated area of the charge process decrease compared with the first discharge process, indicating that a portion of capacity is lost during the subsequent charge process. However, the result that the CV curves are quite similar after the first cycle suggests that the performance of the hierarchically hollow $ZnSn(OH)_6$ and Zn_2SnO_4 nanosphere electrodes are stable.

Table 2. Comparisons between the hierarchically Zn_2SnO_4 hollow nanospheres and previously reported Zn_2SnO_4 structures.

Electrode materials	Reversible capacity (mAh/g)	Current density (mA/g)	Cycle number (n)	Ref.
Zn_2SnO_4 nanoparticles	342	100	40	12
Zn_2SnO_4 cube	420	50	30	13
Zn_2SnO_4 hollow box	540	300	45	14
Zn_2SnO_4/C	563	60	40	12
Zn_2SnO_4/PPY	478.4	60	50	17
Zn_2SnO_4/graphene	326	50	40	18
Zn_2SnO_4/ZIF	349.2	500	20	19
Zn_2SnO_4/PANI	491.0	600	50	20
Flower-like Zn_2SnO_4	501	300	50	24
Zn_2SnO_4 nanoplates	470	120	50	16
Our work	602.5	100	60	
(hierarchical Zn_2SnO_4	470.3	500	60	
hollow nanospheres)	442.8	1000	60	

Conclusions

In summary, the hydrothermal synthesis of hierarchical $ZnSn(OH)_6$ hollow nanospheres and their conversion into hierarchical Zn_2SnO_4 hollow nanospheres (via subsequent calcinations) has been achieved. The former can maintain a reversible specific capacity of 801.2 mAh g^{-1} after 60 cycles, while the latter could retain at 602.5 mAh g^{-1} after 60 cycles at 100 mA g^{-1}. It is note that even if its current density was set as high as 1A g^{-1}, they still could maintain reversible specific capacity of 741.9 mAh g^{-1} (after 1000 cycles) and 442.8 mAh g^{-1} (after 60 cycles), respectively. The present strategy provide a feasible and effective way for the achievement of enhanced cycling performance and rate capability of electrode materials that are subject to large volume changes. The facile synthesis, high specific capacity, good cycling stability and high rate performance of the as-obtained hierarchical $ZnSn(OH)_6$ and Zn_2SnO_4 hollow nanospheres enable them to be promising and competitive high-performance anodes for LIBs.

Notes and references

[a]*Key Laboratory of Colloid & Interface Chemistry (Shandong University), Ministry of Education and School of Chemistry and Chemical Engineering, Shandong University, Jinan 250100, China*
Fax: (+) +86-53188364543; Tel: (+) +86-53188364543
E-mail: xulq@sdu.edu.cn

† Electronic Supplementary Information (ESI) available: [details of any supplementary information available should be included here]. See DOI: 10.1039/b000000x/

‡ This research is financial support by the 973 Project of China (No. 2011CB935901), the National Nature Science Foundation of China and Academy of Sciences large apparatus United Fund (Nos.11179043 and 21471091).

References

1 M.V. Reddy, G.V. Subba Rao, B.V. R. Chowdari, *Chem. Rev.*, 2013, **113**, 5364-5457.

2 J. Hu, M. Chen, X. S. Fang, L. M. Wu, *Chem. Soc. Rev*. 2011, **40**, 5472-5491.

3 X. W. Lou, Y. Wang, C. Yuan, J. Y. Lee, L. A. Archer, *Adv. Mater.* 2006**, 18**, 2325-2329.

4 X. Wang, X. L. Wu, Y. G. Guo, Y. T. Zhong, X. Q. Cao, Y. Ma, J. N. Yao, *Adv. Func. Mater*. 2010**, 20**, 1680-1686.

5 A. Q. Pan, H. B. Wu, L. Zhang, X. W. (David) Lou, *Energy Environ. Sci*. 2013, **6**, 1476-1479.

6 H. K. Wang, A. L. Rogach, *Chem. Mater*. 2014, **26(1)**, 123-133.

7 L. Li, K. H. Seng, Z. X. Chen, Z. P. Guo, H. K. Liu, *Nanoscale* 2013, **5**, 1922-1928.

8 A. M. Cao, J. S. Hu, H. P. Liang, L. J. Wan, *Angew. Chem. Int. Ed.* 2005, **44**, 4391-4395.

9 Y. Wang, Q. S. Zhu, L. Tao, X. W. Su, *J. Mater. Chem*. 2011, **21**, 9248-9254.

10 J. X. Zhu, Z. Y. Yin, D. Yang, T. Sun, H. Yu, H. E. Hoster, H. H. Hng, H. Zhang, Q. Y. Yan, *Energy Environ.Sci*. 2013, **6**, 987-993.

11 Z. Chen, M.H. Cao, C.W. Hu, *J. Phys. Chem*. C. 2011, **115**, 5522-5529.

12 W. S. Yuan, Y. W. Tian, L. J. Liu, J. Z. Li, *Trans. Nonferrou Met. Soc. China*. 2012, **22**, 858-864.

13 N. Feng, S. L. Peng, X. L. Sun, L. Qiao, X. W. Li, P. Wang, D. K. Hu, D. Y. He, *Mater. Letter*. 2012, **76**, 66-68.

14 Y. Zhao, Y. Huang, Q. F. Wang, K. Wang, L. Wang, M. Zong, *RSC Adv*. 2013**, 3 (34)**, 14480-14485.

15 P. Cai, D. K. Ma, Q. C. Liu ,S .M. Zhou ,W. Chen, S. M. Huang, *J. Mater. Chem. A.* 2013, **1**, 5217-5223.

16 C. T. Cherian, M. R. Zheng, M. V. Reddy, B. V. R. Chowdari, and C. H. Sow, *ACS Appl. Mater. Interfaces.* 2013, **5**, 6054-6060.

17 K. Wang, Y. Huang, T. Z. Han, Y. Zhao, H. J. Huang, L. L. Xue, *Ceramics International*. 2013, **40 (1)**, 2359-2364.

18 W. T. Song, J. Xie, S. Y. Liu, G. S. Cao, T. J. Zhu, B. Xin, *J. Mater. Res.* 2012, **27**, 3096-3102.

19 X. Z. Zheng, Y. F. Li, Y. X. Xu, Z. S. Hong, M. D. Wei, *CrystEngComm*, **2012**, *14*, 2112-2116.

20 Y. Zhao, Y. Huang, L. L Xue, X. Sun, Q. F. Wang, W. Zhang, K. Wang, M. Zong, *Polymer Testing*. 2013, **32**, 1582-1587.

21 X. L. Fu, X. X. Wang, Z. X. Ding, Dennis Y. C. Leung, Z. Z. Zhang, J. L. Long, W. X. Zhang, Z. H. Li, X. Z. Fu, *Applied Catalysis B: Environmenta*. 2009, **91**, 67-72.

22 T. Brezesinski, J. Wang, S. H. Tolbert, B. Dunn, *Nature Mater.* 2010, **9**, 146-151.

23 Y.G. Wang, Z.S. Hong, M.D. Wei, Y.Y. Xia, *Adv. Funct. Mater.* 2012, **22**, 5185–5193.

24 J.-Y. Shin, D. Samuelis, J. Maier. *Adv. Funct. Mater*. 2011, **21**, 3464–3472.

25. S. Chen, Y. Xin, Y. Zhou, F. Zhang, Y. Ma, H. Zhou, L.M. Qi, *J. Mater. Chem.* A, 2014, DOI: 10.1039/C4TA03218G

26 C. N. He, S. Wu, N. Q. Zhao, C. S. Shi, E. Z. Liu, J. J. Li, *ACS Nano*, 2013, **7**, 4459-4469

27 Y. J. Fu, X. W. Li, X. L. Sun, X. H. Wang, D. Q. Liu, D. Y. He, *J. Mater. Chem.*, 2012, **22,** 17429-17431.

28 J. Liu, H. Xia, D. F. Xue, L. Lu, *J. Am. Chem*. Soc. 2009, **131**, 12086-12087.

29 J. Liu, Y.C. Zhou, J. B. Wang, Y. Pan, D. F. Xue, *Chem. Commun*. 2011, **47**, 10380-10382.

30 R. R. Zhang, Y.Y. He, A.H. Li, L.Q. Xu, *Nanoscale*, 2014, DOI: 10.1039/C4NR03228D

31 A. Rong, X. P. Gao, G. R. Li, T. Y. Yan, H. Y. Zhu, J. Q. Qu, D. Y. Song, *J. Phys. Chem.* B, 2006, **110**, 14754-14760.